Reduced Order Identification of Aeroelastic Systems with Constrained and Imposed Poles

Hugo Fournier, Paolo Massioni, Minh Tu Pham, Laurent Bako, Robin Vernay

Reduced Order Identification of Aeroelastic Systems with Constrained and Imposed Poles

Hugo Fournier *
Airbus Operations SAS, 31060 Toulouse, France and INSA Lyon, F-69100 Villeurbanne, France

Paolo Massioni† and Minh Tu Pham‡
Univ Lyon, INSA Lyon, Université Claude Bernard Lyon 1, Ecole Centrale de Lyon, CNRS, Ampère, UMR5005, 69621 Villeurbanne, France

Laurent Bako §
Univ Lyon, Ecole Centrale de Lyon, INSA Lyon, Université Claude Bernard Lyon 1, CNRS, Ampère, UMR5005, 69130 Ecully, France

Robin Vernay ¶
Airbus Operations SAS, 31060 Toulouse, France

This work investigates the identification of reduced-order state-space models from aeroelastic simulations of the interaction of a built-in structural finite-element model and a linear aerodynamic model using unsteady potential theory. The objective is to propose and compare different new frequency-based identification methods operating on frequency response associated to the inputs and ouputs of interest. The first methods considered are the Loewner interpolation method and a subspace algorithm. Subsequently, the paper introduces the possibility to apply stability constraints and to impose a certain number of poles estimated beforehand by p-k method, in order to make the identified models closer to the true aeroelastic physics. In order to achieve this goal, new dedicated techniques are developed, and subsequently validated on data generated by random state-space models of various orders, and then using aeroelastic data obtained from structural and aerodynamic aircraft models.

Nomenclature

n	=	Order of the identified state-space model
$\bar{n}$	=	Number of imposed poles
N_y	=	Number of outputs
N_u	=	Number of inputs

*(Corresponding author) PhD Candidate, Flight Physics Department, Loads and Aeroelasticity Engineering, hugo.h.fournier@airbus.com
†Associate Professor
‡Associate Professor
§Associate Professor
¶Research and Development Engineer, Flight Physics Department, Loads and Aeroelasticity

N	=	Number of frequency data samples
V	=	True aircraft speed
M	=	Aircraft Mach number
M_{hh}, B_{hh}, K_{hh}	=	Modal mass, damping and stiffness matrices
Q_{hh}, Q_{vh}	=	Generalized aerodynamic modal and turbulent forces
H_y	=	Output transfer function
$\boldsymbol{h}$	=	Generalized modal coordinates
$\bar{q}$	=	Dynamic pressure
$\boldsymbol{v}$	=	Wind velocity
ω	=	Angular frequency
κ	=	Reduced frequency
$\left[\omega_i, H(e^{j\omega_i})\right]_{i=1\ldots N}$	=	Frequency data
A, B, C, D	=	State-space model matrices
$\boldsymbol{x}, \boldsymbol{u}, \boldsymbol{y}$	=	State, input and output vectors
k	=	Discrete time
V, Σ, W	=	Singular value decomposition of a matrix
$\hat{O}$	=	Estimate of the observability matrix
$\overline{O}$	=	Estimate of the observability matrix, with first N_y rows truncated
$\underline{O}$	=	Estimate of the observability matrix, with last N_y rows truncated
$\mathbb{L}$	=	Loewner matrix
$\mathbb{L}_\sigma$	=	Shifted Loewner matrix
$\lambda_i, \boldsymbol{p_i}$	=	Pole (eigenvalue) and eigenvector
$\bar{\Lambda}$, $\bar{P}$	=	Matrices of imposed poles and of associated eigenvectors
Λ, P	=	Matrices of free poles and of associated eigenvectors
$\mathcal{D}^{\alpha,\beta}$	=	Set of constrained poles location

I. Introduction

The aeroelastic modeling of aircraft dates back to the middle of the twentieth century, where the equations of flight dynamics started including corrections due to quasi-steady interaction between the rigid motion and aerodynamics [1, 2]. With the development of computer capabilities, more advanced techniques based on Computational Fluid Dynamics (CFD) methods allowed to model the aerodynamics with better accuracy, taking into account the full aircraft geometry and using nonlinear, unsteady theory that can capture transonic effects. However, performing such accurate aeroelastic

simulations is a computationally expensive task. Many applications, including dynamical loads computations, flight dynamics simulations, controller synthesis and stability analysis, require a reduced aeroelastic model that takes less time to evaluate. A popular approach consists in generating time-domain data of the Generalized Aerodynamic Forces (GAF) obtained by CFD computations and derive a nonlinear model that can be coupled with structural dynamics to obtain a reduced aeroelastic model [3]. Several techniques exist, including Volterra theory [4, 5], Proper Orthogonal Decomposition (POD) [6–8], Harmonic Balance (HB) method [9] or more recently neural-network-based models [10]. Specific techniques must be developed to reduce the number of high-fidelity CFD computations that must be performed to generate the time data [6, 11]. These techniques are well suited for simulation and analysis. When considering flight dynamics of flexible aircraft, Lagrange equations are generally used and can be simplified by an accurate choice of reference axis. The literature [12–14] has also often made use of mean axes, with respect to which the linear and angular momenta associated with structural vibrations are zero. The work in [15] proposed instead a formulation with an arbitrary choice of body axes.

In their original formulation, the methods cited above lead to nonlinear models that can be used for simulations of a large class of aircraft including very flexible aircraft with large aeroelastic deflections [16, 17]. For controller design, a linear model is often preferred because of the availability of synthesis and analysis tools based on frequency analysis. Gust Load Alleviation (GLA) [18, 19] and active flutter suppression [20] are typical active research topics that are often based on linear models. If a trim equilibrium of the aircraft has been computed using nonlinear techniques, one can make the hypothesis of small displacements and deflections around this point such as done in [21, 22], allowing to define linear structural dynamics of the incremental displacements. By further assuming that the aerodynamics are linear (assuming for instance low angle-of-attack and control surfaces deflections), GAF which are proportional to the modal displacements can be computed using CFD, or faster (but less accurate) techniques such as Doublet Lattice Method (DLM) [23, 24], which works in frequency domain, or its time-domain counterpart Unsteady Lattice Vortex Method (UVLM) [25] used for instance in [26, 27]. Both the DLM and UVLM are based on unsteady potential theory that leads to GAF proportional to the modal displacements, hence can easily be coupled with a structural model obtained by built-in Finite Element Method (FEM) for example. Using DLM leads to GAF computed at different frequency values, based on which LTI models can be identified thanks to Roger [28] or Karpel [29] approximation that fit a transfer function composed of a second-order polynomials and of delay terms from data, like in [30]. Another popular method is the Eigensystem Realization Algorithm (ERA) [31] that identifies a state-space model based on time-data, used by several studies on active flutter suppression [30, 32–34]. With the assumptions of small displacements around a trim equilibrium and linear aerodynamics, linear aeroelastic models can be obtained with this procedure.

Aeroelastic models obtained by GAF rationalization maintain the physical interpretation of the states, which can be assimilated as modal displacements and aerodynamic delays for example. However, in absence of dedicated methods to reduce their order, these models can be prohibitive for numerically intensive control synthesis techniques. From the

authors' experience, classical reduction techniques, such as the balanced truncation, [35], lead to poor approximation of the initial model when the latter is of very high order and numerically ill-conditioned. The current work studies a different strategy, by working directly on identification of the full aeroelastic transfer function, instead of the GAF. The frequency response of the aeroelastic transfer function is first evaluated at different frequencies, and Multi-Input Multi-Output (MIMO) identification algorithms based on this data are used to directly obtain reduced order state-space models. Aerodynamics are modeled by DLM to directly obtain GAF in the frequency domain, and a built-in FEM model is used for structural dynamics. By focusing on the response corresponding to the inputs and outputs of interest, only the main features are modeled, leading to much lower orders than with the classical approach. However, the dependence on the flight parameters (such as Mach and altitude) is lost, and a model must be obtained for each condition separately.The subspace identification is a state-of-the-art set of techniques for estimating a MIMO state-space from time or frequency data, an overview can be found in [36]. The Loewner method [37, 38] is another promising approach, based on rational interpolation theory. In absence of stability constraints, there is no guarantee that these methods will produce models which reflect the stability of the true system, especially when its order is not known in advance. This difficulty, acknowledged in [39] for example, is a typical flaw of the black-box approach, which loses the physical interpretability of the aeroelastic system whose poles are not exactly modeled. The first step to cope with this issue is to impose stability of the identified model. This is done in this work by using the results of [40] based on [41, 42], in which a subspace-based identification is proposed with a general set of constraints imposed to the poles, that includes the constraint of stability. The second step to improve the physical interpretability of the models consists in imposing a set of known aeroelastic poles that have been estimated beforehand by p-k method [43] for example, while other poles are left as free parameters to improve the approximation accuracy. With this hybrid method, the objective is to ensure the stability of the mathematical poles that help approximating the true transfer function, while imposing that some poles of interest are correctly modeled, with direct applications in GLA and active flutter suppression syntheses, but also in effective aeroelastic simulations. Specific techniques are developed based on the subspace identification and inspired by [44], to impose poles with and without constraints on the additional poles.

The contributions of this work are the following:

- A low-order identification approach based on the aeroelastic transfer function frequency response is studied, and the comparison of the Loewner method and subspace methods with and without stability constraints is performed.
- Novel hybrid identification techniques are presented, in which a part of the poles is imposed and the other part is left as free parameters. The possibility to impose constraints on the free poles is investigated. These methods are validated and compared using data generated from fixed-order random state-space models, before being applied to aeroelastic data obtained from FEM and DLM models.

Section II presents the objective of identifying a reduced-order state-space model that represents an aeroelastic model. In section III two MIMO identification algorithms based on frequency data are presented: the Loewner interpolation

method, and a subspace algorithm. Section IV uses the same subspace framework with additional constraints on the poles location, and section VI investigates methods for imposing known poles to the identified model, with and without constraints on the free poles. Finally section VII presents the results of the validation and comparison of the presented methods on different sets of data. A summary of the techniques presented in this work and their main characteristics can be found in Table 1 in the results section, to help the reader keep track of the different methods.

II. Objective: Aeroelastic reduced order modeling

We consider the following equations describing a linearized aeroelastic system, that results from the interaction of a structural model and an aerodynamic model [1]:

$$M_{hh}\ddot{\boldsymbol{h}} + B_{hh}\dot{\boldsymbol{h}} + K_{hh}\boldsymbol{h} = \bar{q}\left[Q_{hh}(M,\kappa)\boldsymbol{h} + Q_{uh}(M,\kappa)\boldsymbol{u} + Q_{vh}(M,\kappa)\frac{\boldsymbol{v}}{V}\right] \tag{1}$$

where $\boldsymbol{h}$ is the modal displacement, $\bar{q} = \frac{1}{2}\rho V^2$ is the dynamic pressure with ρ the air density and V the aircraft true air speed, M_{hh} is the modal mass matrix, B_{hh} is the modal damping matrix, K_{hh} the modal stiffness matrix, Q_{hh}, Q_{uh} and Q_{vh} are the modal aerodynamic forces due to modal displacements $\boldsymbol{h}$, control surfaces displacements $\boldsymbol{u}$ and wind velocity $\boldsymbol{v}$ respectively. The computation is performed at different Mach numbers M and reduced frequencies $\kappa = \frac{\omega b}{V}$ with b the reference semi-chord and ω the angular frequency. This formulation includes the case where the structure and inertia of the aircraft are modeled by a finite elements model (FEM) and the aerodynamics are modeled by a linear unsteady potential theory, using for example Doublet Lattice Method (DLM) [23, 24]. From the structural, inertial and aerodynamic models, an aeroelastic solver such as sol145 of Nastran can be used to compute the matrices defining Eq. (1). Output variables of interest (integrated loads, displacements, load factors, etc) can then be obtained based on the values of $\boldsymbol{h}$, $\boldsymbol{u}$ and $\boldsymbol{v}$:

$$\boldsymbol{y} = H_y(s)\begin{bmatrix}\boldsymbol{h}^T & \boldsymbol{u}^T & \boldsymbol{v}^T\end{bmatrix}^T \tag{2}$$

where $s = j\omega$ and $j^2 = -1$.

Because of the dependence of the generalized forces Q_{hh}, Q_{uh} and Q_{vh} on the angular frequency, the aeroelastic transfer function is not rational and cannot be transformed into a state-space model. In order to approximate it with a state-space model, one must perform a system identification based on data. This is classically done by first approximating the aerodynamic forces with rational functions expressed as the sum of a second order polynomial and a delay term, using for example Roger [28] or Karpel [29] methods. A realization algorithm such as ERA [31] is sometimes used to identify the aerodynamic forces, from time data.

This method can lead to very high-order models, which can be used for simulations but not for computationally intensive applications such as controller synthesis. In particular, Active Flutter Suppression (AFS) and Gust Load

Alleviation (GLA) require low-order models that represent the aeroelastic physics with good fidelity and include a high number of modes. Such models can be obtained by evaluating the frequency response of the full aeroelastic transfer function defined by Eq. (1) and (2) and then identifying a model based on these frequency data. The value of the transfer functions from inputs $\boldsymbol{u}$ and $\boldsymbol{v}$ to output $\boldsymbol{y}$ can be calculated at different frequencies and Mach numbers by evaluating the aerodynamic force matrices at these frequencies and taking the Laplace transform of the left-hand side of Eq. (1). The frequency data response is noted $\left[H(e^{j\omega_i})\right]_{i=1\dots N} \in \mathbb{C}^{N_y \times N_u}$ where N_y is the number of output, N_u is the number of input, including the different control surfaces deflection angles and the wind velocity, and N is the number of frequencies at which the response is computed.

From noiseless frequency data $\left[H(e^{j\omega_i})\right]_{i=1\dots N}$, the objective is then to identify a state-space model of fixed order n of the form:

$$\begin{cases} \boldsymbol{x}_{k+1} = A\boldsymbol{x}_k + B\boldsymbol{u}_k \\ \boldsymbol{y}_k = C\boldsymbol{x}_k + D\boldsymbol{u}_k \end{cases} \tag{3}$$

where k is the discrete time, $\boldsymbol{x}$ is the state vector, $\boldsymbol{u}$ and $\boldsymbol{y}$ are respectively the input and output vectors, and the matrices $A \in \mathbb{R}^{n\times n}$, $B \in \mathbb{R}^{n\times N_u}$, $C \in \mathbb{R}^{N_y\times n}$ and $D \in \mathbb{R}^{N_y\times N_u}$ are matrices defining the model. A continuous-time state-space model can equivalently be obtained. Note that this model is valid for given mass configuration of the aircraft and aerodynamic conditions (Mach and altitude for example).

This work investigates the possibility to constrain the identified model to make its behavior closer to the true physical system. Indeed, the existing MIMO identification techniques from frequency data will generally lead to identified poles that differ from the true aeroelastic poles. The most obvious effect comes from the fact that even when the true system is stable, the identified model can be unstable, hence improper not only for simulations as the time response will diverge, but also for controller synthesis where the stabilization of the system will be a strong, unjustified, additional constraint. Another undesired effect of the bad identification of the aeroelastic poles is the fact that the physical interpretability is lost. For example, when studying the evolution of an unstable pole (flutter) and the design of its active stabilization, one wants to be sure that it is correctly represented by the model, which motivates the development of identification with constraints on the poles location, and with some known aeroelastic poles imposed to the identified state-space model. This has a direct influence on the fields of GLA and active flutter suppression, but possibly other disciplines can take advantage of this approach.

The poles imposed during the identification can be obtained from a reliable (possibly high-order) model, using for example GAF rationalization as presented in the introduction. The p-k method introduced in [43] can provide a good estimation of the poles of the aeroelastic system, associated to structural modes that have been modified by the unsteady aerodynamic effect. It works through an iterative process based on the matrices M_{hh}, B_{hh}, K_{hh} and Q_{hh}, at different values of the aircraft velocity for a given Mach number.

III. State-of-the-art: identification of a MIMO state-space model from frequency data

A. Subspace identification method

The idea of subspace methods is to find a realization of some data, namely to define a family of states that mathematically describes the data, without necessarily having a physical interpretation. The term "subspace" comes from the fact that a reduced number of states is wanted, leading to the search of low-dimensional subspaces in which the states evolve. This section presents a subspace algorithm proposed by McKelvey and Ljung in [45]. Techniques developed in sections V and VI are based on this method.

Consider the discrete Laplace transform of the state-space model of Eq. (3) that is assumed to model the data:

$$\begin{cases} e^{j\omega}\boldsymbol{X}(j\omega) = A\boldsymbol{X}(j\omega) + B\boldsymbol{U}(j\omega) \\ \boldsymbol{Y}(j\omega) = C\boldsymbol{X}(j\omega) + D\boldsymbol{U}(j\omega) \end{cases} \tag{4}$$

where $\boldsymbol{X}, \boldsymbol{U}$ and $\boldsymbol{Y}$ are the Laplace transforms of the state $\boldsymbol{x}$, input $\boldsymbol{u}$ and output $\boldsymbol{y}$ respectively. A unitary sampling time has been assumed without loss of generality. When considering the impulse response of this system at $q \geq n$ consecutive discrete sampling times, the following equation is obtained assuming that the data H have been generated by the state-space model of Eq. (3):

$$\begin{bmatrix} H(e^{j\omega}) \\ e^{j\omega}H(e^{j\omega}) \\ \vdots \\ e^{(q-1)j\omega}H(e^{j\omega}) \end{bmatrix} = \mathcal{O}X^C(j\omega) + \Gamma \begin{bmatrix} I_{N_u} \\ e^{j\omega}I_{N_u} \\ \vdots \\ e^{(q-1)j\omega}I_{N_u} \end{bmatrix} \tag{5}$$

where H is the frequency response of the system, the compound state matrix is defined as

$$X^C(j\omega) = \begin{bmatrix} \boldsymbol{X}^1(j\omega) & \boldsymbol{X}^2(j\omega) & \dots & \boldsymbol{X}^{N_u}(j\omega) \end{bmatrix} \in \mathbb{C}^{n \times N_u} \tag{6}$$

where $\boldsymbol{X}^i(j\omega)$ is the response of $\boldsymbol{X}(j\omega)$ to an impulse at input i. The matrix $\mathcal{O}$ is a generalized observability matrix defined as

$$\mathcal{O} = \begin{bmatrix} C \\ CA \\ \vdots \\ CA^{q-1} \end{bmatrix} \in \mathbb{R}^{qN_y \times n} \tag{7}$$

The matrix Γ is the lower triangular block-Toeplitz matrix associated to the Markov parameters, and is defined as:

$$\Gamma = \begin{bmatrix} D & 0 & \dots & \dots & 0 \\ CB & D & 0 & & \vdots \\ CAB & CB & D & \ddots & \vdots \\ \vdots & \vdots & \vdots & \ddots & 0 \\ CA^{q-2}B & CA^{q-3}B & CA^{q-4}B & \dots & D \end{bmatrix} \in \mathbb{C}^{qN_y \times qN_u} \tag{8}$$

When evaluating Eq. (5) at N different frequencies $(\omega_i)_{i=1\dots N}$, the following equation is obtained:

$$\mathcal{H} = \mathcal{O}\mathcal{X}^C + \Gamma\mathcal{U} \tag{9}$$

with

$$\mathcal{X}^C = \begin{bmatrix} X^C(j\omega_1) & X^C(j\omega_2) & \dots & X^C(j\omega_N) \end{bmatrix} \in \mathbb{C}^{n \times N_u N} \tag{10}$$

$$\mathcal{H} = \begin{bmatrix} H(e^{j\omega_1}) & H(e^{j\omega_2}) & \dots & H(e^{j\omega_N}) \\ e^{j\omega_1}H(e^{j\omega_1}) & e^{j\omega_2}H(e^{j\omega_2}) & \dots & e^{j\omega_N}H(e^{j\omega_N}) \\ \vdots & \vdots & \ddots & \vdots \\ e^{(q-1)j\omega_1}H(e^{j\omega_1}) & e^{(q-1)j\omega_2}H(e^{j\omega_2}) & \dots & e^{(q-1)j\omega_N}H(e^{j\omega_N}) \end{bmatrix} \in \mathbb{C}^{qN_y \times NN_u} \tag{11}$$

and

$$\mathcal{U} = \begin{bmatrix} I_{N_u} & I_{N_u} & \dots & I_{N_u} \\ e^{j\omega_1}I_{N_u} & e^{j\omega_2}I_{N_u} & \dots & e^{j\omega_N}I_{N_u} \\ \vdots & \vdots & \ddots & \vdots \\ e^{(q-1)j\omega_1}I_{N_u} & e^{(q-1)j\omega_2}I_{N_u} & \dots & e^{(q-1)j\omega_N}I_{N_u} \end{bmatrix} \in \mathbb{C}^{qN_u \times NN_u} \tag{12}$$

The objective of such a formulation is to obtain from data the value of a generalized observability matrix of the system. This can be achieved by multiplying equation Eq. (9) from the right by an operator $\mathcal{U}^\perp$ that projects onto the null space of $\mathcal{U}$. It can be obtained as

$$\mathcal{U}^\perp = I - \mathcal{U}^T(\mathcal{U}\mathcal{U}^T)^{-1}\mathcal{U} \tag{13}$$

Eq. (9) then becomes

$$\mathcal{H}\mathcal{U}^\perp = \mathcal{O}\mathcal{X}\mathcal{U}^\perp \tag{14}$$

An estimate of the observability matrix of the system can be obtained by performing a singular value decomposition (SVD) of $\mathcal{H}\mathcal{U}^{\perp}$ and keeping only the right orthogonal vectors associated to the first n singular value, which is, by writing:

$$\mathcal{H}\mathcal{U}^{\perp} = V\Sigma W^{*} \tag{15}$$

where Σ has the singular values on its diagonal and zeros elsewhere, V and W are unitary matrices ($VV^{*} = I$, $WW^{*} = I$), the superscript * representing the hermitian transpose. The matrix $\hat{O} \in \mathbb{C}^{nN_y \times n}$ defined as the first n columns of V is then an estimate of the observability matrix of the system. Note that in order to obtain a real estimate of the observability matrix, one must replace $\mathcal{H}$ by $[Re(\mathcal{H}), Im(\mathcal{H})]$ and similarly for $\mathcal{U}$ and $\mathcal{X}$ in Eq. (9).

Once an estimate $\hat{O}$ of the observability matrix for a certain realization of the state-space model has been computed, the corresponding matrix C is obtained as the first N_y rows as seen in the definition of the observability matrix in Eq. (7) and the matrix A is obtained as:

$$A = \underline{O}^{\dagger}\overline{O} \tag{16}$$

where $\underline{O}$ and $\overline{O}$ are the matrices obtained by removing the last and first N_y rows of $\hat{O}$ respectively, and the superscript † denotes the Moore-Penrose pseudo-inverse.

When the matrices A and C are known, the dependence of the state-space's transfer function on matrices B and D is linear, they can be obtained as the solution of the following linear least square problem:

$$\min_{B,D} \sum_{i=1}^{N} \left\| C\left[e^{j\omega_i} I_N - A\right]^{-1} B + D - H(e^{j\omega_i}) \right\|_F^2 \tag{17}$$

where $\|.\|_F$ denotes the Frobenius norm. This problem admits the following solution:

$$\begin{bmatrix} B \\ D \end{bmatrix} = \begin{bmatrix} M \\ \overline{M} \end{bmatrix}^{\dagger} \begin{bmatrix} Z \\ \overline{Z} \end{bmatrix} \tag{18}$$

where $\overline{M}$ and $\overline{Z}$ are the complex conjugates of M and Z respectively, which in turn are defined as

$$M = \begin{bmatrix} C\left[e^{j\omega_1} I_N - A\right]^{-1} & I_{N_y} \\ \vdots & \vdots \\ C\left[e^{j\omega_N} I_N - A\right]^{-1} & I_{N_y} \end{bmatrix} \in \mathbb{C}^{NN_y \times (n+N_y)} \tag{19}$$

and

$$Z = \begin{bmatrix} H(e^{j\omega_1}) \\ \vdots \\ H(e^{j\omega_N}) \end{bmatrix} \in \mathbb{C}^{NN_y \times N_u} \tag{20}$$

With the matrices A, B, C and D defining the identified discrete-time state-space model with a unitary sampling time.

B. Loewner method

This section presents another identification approach for MIMO systems based on frequency data, the Loewner method [37, 38]. With this technique, a continuous-time state-space model is identified. This method comes from the field of rational interpolation, and it looks for a state-space which perfectly matches the frequency data, as a first step. A reduction based on singular value decomposition is then performed, leading to a reduced-order model that approximates the data. The Loewner method is well suited to noiseless data. In the following, only the procedure is described, in the particular case in which the data directions are defined by the canonical bases of the input and output spaces.

In the Loewner method, the frequency response data $\left[H(e^{j\omega_i})\right]_{i=1\ldots N}$ is first split in two subsets of data associated to the left ω^l and right ω^r frequency sets:

$$\left[\omega_i, H(e^{j\omega_i})\right]_{i=1\ldots N} \quad \rightarrow \quad \left[\omega_i^l, H(e^{j\omega_i^l})\right]_{i=1\ldots N^l} \cup \left[\omega_i^r, H(e^{j\omega_i^r})\right]_{i=1\ldots N^r} \tag{21}$$

To the authors' knowledge, there is no clear study of the optimal way to split the data into two subsets in the literature. These sets are used to create the Loewner matrix:

$$\mathbb{L} = \begin{bmatrix} \frac{H(e^{j\omega_1^l}) - H(e^{j\omega_1^r})}{\omega_1^l - \omega_1^r} & \cdots & \frac{H(e^{j\omega_1^l}) - H(e^{j\omega_{N^r}^r})}{\omega_1^l - \omega_{N^r}^r} \\ \vdots & \ddots & \vdots \\ \frac{H(e^{j\omega_{N^l}^l}) - H(e^{j\omega_1^r})}{\omega_{N^l}^l - \omega_1^r} & \cdots & \frac{H(e^{j\omega_{N^l}^l}) - H(e^{j\omega_{N^r}^r})}{\omega_{N^l}^l - \omega_{N^r}^r} \end{bmatrix} \in \mathbb{C}^{N^l N_y \times N^r N_u} \tag{22}$$

and the shifted Loewner matrix:

$$\mathbb{L}_\sigma = \begin{bmatrix} \frac{\omega_1^l H(e^{j\omega_1^l}) - \omega_1^r H(e^{j\omega_1^r})}{\omega_1^l - \omega_1^r} & \cdots & \frac{\omega_1^l H(e^{j\omega_1^l}) - \omega_{N^r}^r H(e^{j\omega_{N^r}^r})}{\omega_1^l - \omega_{N^r}^r} \\ \vdots & \ddots & \vdots \\ \frac{\omega_{N^l}^l H(e^{j\omega_{N^l}^l}) - \omega_1^r H(e^{j\omega_1^r})}{\omega_{N^l}^l - \omega_1^r} & \cdots & \frac{\omega_{N^l}^l H(e^{j\omega_{N^l}^l}) - \omega_{N^r}^r H(e^{j\omega_{N^r}^r})}{\omega_{N^l}^l - \omega_{N^r}^r} \end{bmatrix} \in \mathbb{C}^{N^l N_y \times N^r N_u} \tag{23}$$

Additionally, the following matrices are defined:

$$F = \begin{bmatrix} H(e^{j\omega_1^l}) \\ \vdots \\ H(e^{j\omega_{N^l}^l}) \end{bmatrix} \in \mathbb{C}^{N^l N_y \times N_u} \tag{24}$$

and

$$G = \begin{bmatrix} H(e^{j\omega_1^r}) & \dots & H(e^{j\omega_{N^r}^r}) \end{bmatrix} \in \mathbb{C}^{N_y \times N^r N_u} \tag{25}$$

The following singular value decomposition of the horizontally appended Loewner and shifted Loewner matrices is then performed

$$\begin{bmatrix} \mathbb{L} & \mathbb{L}_\sigma \end{bmatrix} \approx V \Sigma_l \tilde{W}^* \tag{26}$$

where only the first n singular values are kept, which will define the order of the identified state-space model. The value of n can be taken as the rank of the Loewner matrix $\mathbb{L}$. In this case, assuming enough data are available, it defines the McMillan degree of the system [37] which is the order of a minimal realization in case the system is causal. Practically, n can be set by the user to identify a reduced-order model. The same is done with the vertically appended matrices:

$$\begin{bmatrix} \mathbb{L} \\ \mathbb{L}_\sigma \end{bmatrix} \approx \tilde{V} \Sigma_r W^* \tag{27}$$

The following matrices can then be recovered:

$$E = -V^* \mathbb{L} W \tag{28}$$

$$A = -V^* \mathbb{L}_\sigma W \tag{29}$$

$$B = V^* F \tag{30}$$

$$C = GW \tag{31}$$

defining the identified continuous-time descriptor state-space model

$$\begin{cases} E\dot{\boldsymbol{x}} = A\boldsymbol{x} + B\boldsymbol{u} \\ \boldsymbol{y} = C\boldsymbol{x} \end{cases} \tag{32}$$

As explained in [46] the D matrix is incorporated in the other matrices defining the descriptor model, and can be

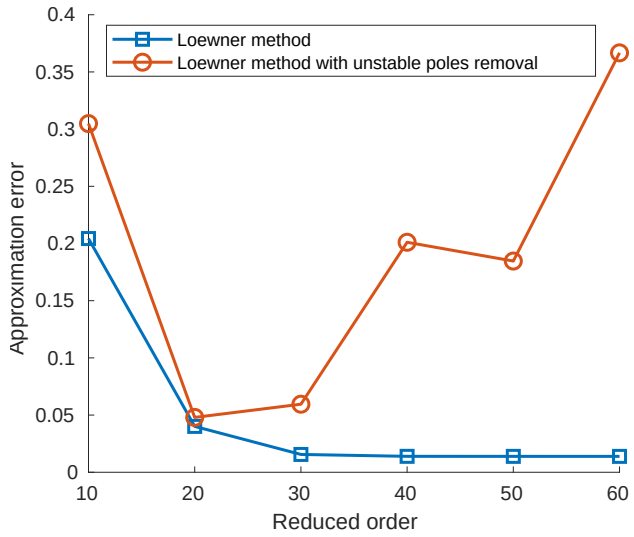

Figure 1 Approximation error with and without unstable poles removal using the Loewner method

extracted from them. To the authors' knowledge, the procedure to recover D has not been accurately described in the literature. We propose a solution in appendix VIII.A in the case the system is causal and does not include integrators. Note that by following the procedure presented above, the matrices defining the model are complex. Real matrices are obtained by splitting the frequency response data H into their real and imaginary parts.

IV. Subspace identification with constraints on the poles

The subspace identification algorithm or the Loewner method described in section III does not ensure the stability of the identified state-space model. Even when the true system is stable, a reduced-order state-space model may contain unstable poles. It will lead to diverging time simulations and can cause problems when used for the design of a controller, for instance. For this reason, it is common to simply remove the unstable poles from the identified model as studied in [47]. This post-analysis can lead to a poor approximation capability when the identified model includes a high number of unstable modes. This is illustrated in Fig. 1 where aeroelastic data have been approximated by models of variable reduced orders obtained by the Loewner method, with and without removing the unstable poles. It can be seen that for an adequate choice of the model's reduced order (20 here), artificially imposing the stability in post-analysis leads to a satisfactory result. However, when increasing the reduced order, the model contains more artificial unstable poles and removing them causes the approximation error to increase. This is not only sub-optimal, but also requires a good a-priori knowledge of the system to obtain a good approximation. This motivates the development of dedicated techniques, in which the stability constraint is part of the identification process, and not imposed a-posteriori.

In [42], an identification algorithm based on subspace methods is developed to impose stability to the state-space model, using convex optimization. The work of [40] proposed a state-space identification algorithm based on convex

optimization in which the location of the poles are constrained in a similar way as done in [41] for H_∞ synthesis. In this section this technique is presented as an introduction to the methods developed in this work.

Starting from an estimate $\hat{O}$ of the observability matrix of the system, the objective is to find matrices A and C that generate an observability matrix close to $\hat{O}$ with eigenvalues of A lying in a region of the following class:

$$\mathcal{D}^{\alpha,\beta} = \left\{ z \in \mathbb{C} \,:\, \alpha + \beta z + \beta^T \overline{z} \succeq 0 \right\} \tag{33}$$

where α is a real symmetric matrix, β is a real square matrix, the $\succeq 0$ notation denotes matrix definite positivity and $\overline{z}$ is the complex conjugate of z. This class includes the unit disk plane and the left half plane to ensure stability of discrete-time and continuous-time systems respectively.

It is shown in [41] that the eigenvalues of a matrix $A \in \mathbb{C}^{n\times n}$ lie within a region $\mathcal{D}^{\alpha,\beta}$ defined in Eq. (33) if and only if there exists a matrix $P \in \mathbb{R}^{n\times n}$ such that $P = P^T \succ 0$ and

$$\alpha \otimes P + \beta \otimes AP + \beta^T \otimes (AP)^T \succeq 0 \tag{34}$$

where the $\otimes$ symbol denotes the Kronecker product.

A matrix A can be obtained by the following optimization problem:

$$\min_{A,P} \left\| \underline{O} AP - \overline{O} P \right\|_F \tag{35}$$

$$\text{subject to} \begin{cases} \alpha \otimes P + \beta \otimes AP + \beta^T \otimes (AP)^T \succeq 0 \\ P = P^T \succ 0 \end{cases} \tag{36}$$

The cost function and the inequality constraint contain a non-convex term AP which can be removed by defining the variable $Q = AP$, leading to the following convex formulation:

$$\min_{Q,P} \left\| \underline{O} Q - \overline{O} P \right\|_F \tag{37}$$

$$\text{subject to} \begin{cases} \alpha \otimes P + \beta \otimes Q + \beta^T \otimes Q^T \succeq 0 \\ P = P^T \succ 0 \end{cases} \tag{38}$$

We can then compute $A = QP^{-1}$ as P is positive definite. The matrix C is then obtained as the first N_y rows of $\hat{O}$, and the matrices B and D can be calculated similarly as in Eq. (17).

V. Hybrid identification: Imposed known poles and unconstrained unknown poles. Subspace identification with orthogonal additional eigenvectors (SIDORT)

This section presents an approach for the hybrid identification of a state-space model, where some poles are imposed and the remaining poles are free parameters. A method to obtain a state-space model whose poles are all known beforehand is described [44]. We generalize this procedure to the case in which some poles are unknown, in order to give additional degrees of freedom to the identification, and better fit to the frequency data. Moreover, in most real-life applications, a small portion of the true system's poles is known, like in the aeroelastic equations presented in section II. An alternative to this method is obtained by working on the parameters defining the MIMO transfer function. This presents two main disadvantages: first, this involves operations on polynomials, that present numerical issues when the order increases. Secondly, by fixing the transfer function order to n, the associated state-space model will be of order $\min(nN_y, nN_u)$ with n distinct poles. For this reason, the transfer function approach will not be applied in the results section.

We start by estimating an observability matrix $\hat{O}$ using the subspace algorithm described in section III.A. We assume that the poles of the system have an algebraic multiplicity of 1. We first impose some poles $(\bar{\lambda}_i)_{i=1\dots\bar{n}}$ and compute the associated eigenvectors by noting that:

$$\hat{O}\bar{\boldsymbol{p}}_{\boldsymbol{i}} = \begin{bmatrix} C\bar{\boldsymbol{p}}_{\boldsymbol{i}} \\ CA\bar{\boldsymbol{p}}_{\boldsymbol{i}} \\ \vdots \\ CA^{n-1}\bar{\boldsymbol{p}}_{\boldsymbol{i}} \end{bmatrix} = \begin{bmatrix} C \\ \bar{\lambda}_i C \\ \vdots \\ \bar{\lambda}_i{}^{n-1} C \end{bmatrix} \bar{\boldsymbol{p}}_{\boldsymbol{i}} \tag{39}$$

For each pole $\bar{\lambda}_i$ a corresponding eigenvector can be found as $\bar{\boldsymbol{p}}_{\boldsymbol{i}} \in \ker(\tilde{O})$ where

$$\tilde{O} = \hat{O} - \begin{bmatrix} C \\ \bar{\lambda}_i C \\ \vdots \\ \bar{\lambda}_i{}^{n-1} C \end{bmatrix} \tag{40}$$

When all the $\bar{n}$ column eigenvectors $\bar{\boldsymbol{p}}_{\boldsymbol{i}}$ have been obtained, they can be assembled into a matrix $\bar{P}$ such that the matrix A verifies

$$A \begin{bmatrix} \bar{P} & P \end{bmatrix} = \begin{bmatrix} \bar{\Lambda} & 0 \\ 0 & \Lambda \end{bmatrix} \begin{bmatrix} \bar{P} & P \end{bmatrix} \tag{41}$$

where $\bar{P}$ and $\bar{\Lambda}$ are known. The objective is to find eigenvalues λ_i and their associated eigenvectors $\boldsymbol{p_i}$ that best approximate the data and such that $\begin{bmatrix} \bar{P} & P \end{bmatrix}$ is invertible.

There is no guarantee that a family of $\bar{n}$ independent vectors $\bar{\boldsymbol{p}}_{\boldsymbol{i}}$ can be found in the null space of $\tilde{O}$, whose dimension can be zero. Vectors $\bar{\boldsymbol{p}}_{\boldsymbol{i}}$ such that $\tilde{O}\bar{\boldsymbol{p}}_{\boldsymbol{i}} \approx \boldsymbol{0}$ can be obtained by the singular value decomposition of $\tilde{O} = V\Sigma W^*$ and taking the last column of W, that is the right vector associated to the minimum singular value. No mention is done in [44] of why the matrix composed of the eigenvectors $\bar{\boldsymbol{p}}_{\boldsymbol{i}}$ should be invertible but for each pole $\bar{\lambda}_i$, if the last column of W does not make the rank of P increase, then the previous column can be used instead and so on, until the assembled matrix has full rank.

By making the assumption that the column vectors $\boldsymbol{p_i}$ that compose the matrix P are orthogonal to the previously imposed $\bar{\boldsymbol{p}}_{\boldsymbol{i}}$, we can find the remaining eigenvectors $\boldsymbol{p_i}$ by decomposing them on a basis of the orthogonal of $\text{span}([\bar{\boldsymbol{p}}_{\boldsymbol{i}}]_{i=1\dots\bar{n}})$. We first obtain such a basis by finding $\boldsymbol{e_i} \in \ker(\bar{P}^*)$ where * is the complex adjoint, by singular value decomposition for example, taking $\boldsymbol{e_i}$ as right column vectors corresponding to singular values equal to zero. Note that this basis is orthogonal, because the right and left matrices of the singular value decomposition are orthogonal. Since $\bar{P}$ is of rank $\bar{n}$ and $\bar{P} \in \mathbb{C}^{n\times\bar{n}}$, there exist exactly $n - \bar{n}$ singular values of $\bar{P}^*$ equal to zero. We look for the coefficients k_{ij} that verify

$$\boldsymbol{p_j} = \sum_{i=1}^{n-\bar{n}} k_{ij}\boldsymbol{e_i} \tag{42}$$

which is, by assembling the vectors $\boldsymbol{e_i}$ and the coefficients k_{ij} into matrices E and K,

$$P = EK \tag{43}$$

with $E \in \mathbb{C}^{n\times(n-\bar{n})}$ and $K \in \mathbb{C}^{(n-\bar{n})\times(n-\bar{n})}$. We then recall from section III that $\underline{O}A = \overline{O}$ hence, after right multiplying by the eigenvector $\boldsymbol{p_j}$, it results in solving the generalized eigenvalues problem

$$\overline{O}E\boldsymbol{k_j} = \lambda_j\underline{O}E\boldsymbol{k_j} \qquad j = 1\dots n-\bar{n} \tag{44}$$

where the $\boldsymbol{k_j}$ are columns of K. Since $\underline{O}$ is full-column-rank, from Sylvester inequality $\text{rank}(\underline{O}E) = \text{rank}(E) = n - \bar{n}$. Hence, this comes down to an eigenvalue problem:

$$\left[\underline{O}E\right]^\dagger \overline{O}E\boldsymbol{k_j} = \lambda_j\boldsymbol{k_j} \qquad j = 1\dots n-\bar{n} \tag{45}$$

the pseudo-eigenvectors $\boldsymbol{p_j}$ are then recovered as $\boldsymbol{p_j} = E\boldsymbol{k_j}$. The matrix $\begin{bmatrix} \bar{P} & P \end{bmatrix}$ is invertible because both $\bar{P}$ and P are full rank and because vectors $\bar{\boldsymbol{p}}_{\boldsymbol{i}}$ are independent of vectors $\boldsymbol{p_i}$ due to the orthogonality constraint. The matrix A can then be computed with Eq. (41), the matrix C is obtained as the first N_y rows of $\hat{O}$, and the matrices B and D can be

calculated similarly as in Eq. (17).

VI. Hybrid identification: Imposed known poles and constrained unknown poles

A. Subspace identification with Pseudo-Eigenvalue problem (SIDPEV)

If the assumption of orthogonality of the unknown eigenvectors is dropped, the matrix P of the generalized eigenvalue problem (39) can be obtained by a non-convex optimization. We first obtain the eigenvectors $\bar{P}$ associated to the imposed poles in a similar way as done in section V. The matrix P associated to the unknown eigenvectors can then be obtained iteratively, by solving the following optimization for each unknown eigenvector successively:

$$\text{For } i = 1 \dots n - \bar{n} \tag{46}$$

$$\min_{\boldsymbol{p_i}, \lambda_i} \left\| \underline{O}^{\dagger} \overline{O} \boldsymbol{p_i} - \lambda_i \boldsymbol{p_i} \right\|_2 \tag{47}$$

$$\text{s.t.} \begin{cases} \text{rank}(\begin{bmatrix} \bar{P} & P_i \end{bmatrix}) = \bar{n} + i \\ \lambda_i \in \mathcal{D}^{\alpha,\beta} \\ \|\boldsymbol{p_i}\| = 1 \end{cases} \tag{48}$$

where $P_i \in \mathbb{C}^{n \times i}$ is the matrix containing the first i eigenvectors computed so far, including the unknown vector $\boldsymbol{p_i}$, and the sets $\mathcal{D}^{\alpha,\beta}$ have been defined in section IV. A constraint $\|\boldsymbol{p_i}\| = 1$ is added to avoid trivial solutions. This optimization problem can be approximated by a Bilinear Matrix Inequality problem by relaxing the rank constraint into a constraint of the type $[\bar{P}\, P_i]^*[\bar{P}\, P_i] > 0$. Otherwise, the problem can be solved by a nonlinear optimization with constraint method, such as the interior-point method [48, 49], with the nonlinear rank constraint expressed as a positive lower bound on the matrix minimum singular value for example. The latter option is preferred for its robustness. It can be seen that the gradient of the objective function with respect to the variables is easily computed. Furthermore, each eigenvalue/eigenvector pair is computed independently, so each optimization problem has low number of variables which makes the method not too computationally intensive.

B. Direct Nonlinear Optimization with Constraints (DNOC)

The methods exposed previously aim at decomposing the general problem of state space model identification with imposed poles and constraints on the unknown poles in a way that limits the computational cost. By doing so, errors due to over-constraining hypotheses or to suboptimal solutions can accumulate and increase the approximation error. Another strategy consists in solving the different steps simultaneously by a single optimization.

A direct identification of a state space model with imposed poles and constraints on the unknown poles can be obtained by looking for the identified model in its modal canonical form and solving the following non-convex

optimization problem with constraints:

$$\min_{\substack{\lambda_i, B, C, D \\ i=1\dots n-\bar{n}}} \sum_{k=1}^{N} \left\| C \left[e^{j\omega_k} I_n - A(\lambda) \right]^{-1} B + D - H(e^{j\omega_k}) \right\|_F^2 \tag{49}$$

$$\text{s.t. } \lambda_i \in \mathcal{D}^{\alpha,\beta} \tag{50}$$

with

$$A(\lambda) = \begin{bmatrix} \Psi(\bar{\lambda}_1) & & & & & \\ & \ddots & & & 0 & \\ & & \Psi(\bar{\lambda}_{\bar{n}}) & & & \\ & & & \Psi(\lambda_1) & & \\ & 0 & & & \ddots & \\ & & & & & \Psi(\lambda_{n-\bar{n}}) \end{bmatrix} \tag{51}$$

and

$$\bar{\Psi}(\lambda) = \begin{bmatrix} Re(\bar{\lambda}) & Im(\bar{\lambda}) \\ -Im(\bar{\lambda}) & Re(\bar{\lambda}) \end{bmatrix} \tag{52}$$

The matrices A, B, C and D are obtained simultaneously, by an interior-point algorithm [48, 49] for example. The computational cost is expected to be higher than with the other methods described above, because of the high number of variables and the non-convexity of the optimization. Because of the non-convex nature of the problem, solvers such as the interior-point method do not guarantee the convergence to a global minimum.

For example, with the above formulation and when only the poles stability is wanted, the free poles must lie within the complex unit circle, and can be parameterized by the modulus and angle, with a constraint on the former. The research space can be reduced to the half plane by looking only to positive imaginary values, and adding the complex conjugate in the matrix A. If a continuous-time model is desired, the poles can be parameterized by their real and imaginary values, imposing the former to have negative values. The research space can also be reduced, by considering poles with frequency not higher than the maximum data frequency. After experimenting with the two approaches, the discrete-time formulation has proved more efficient and will be used in the results section. Note that this nonlinear optimization problem with constraints can be transformed into an unconstrained problem in some cases. In the case of stability of a discrete-time model, the modulus of the unknown poles can be taken as the output of a bijective function $f : \mathbb{R} \to [0, 1]$ such as the sigmoid function. Using initial conditions from the result of a numerically simpler algorithm (like the SIDPEV described in section VI.A) is not advised, as it can correspond to a local minimum. Rather, random

initial conditions close to unity are preferred in this work.

VII. Numerical Results

A. Validation scenarios

The methods described in this paper will be tested in different conditions in the next sections. The objectives that are expected to be fulfilled by the results are the following:

1) Compare the ability to identify a MIMO model of the subspace and the Loewner methods
2) Evaluate the capability to approximate a high-order MIMO model with a variable reduced order model
3) Compare the computational time needed by the different methods to identify models based on the same data
4) Verify that the methods of sections V and VI can exactly impose some known poles

In order to satisfy these objectives, we study two scenarios. In the first one, the so-called "test data" are generated from a fixed-order MIMO state-space model defined by random matrices B, C and D and a matrix A with conjugated poles on its diagonal. The poles have a constant damping ratio and regularly spaced frequencies. Each pole is simple (algebraic multiplicity equal to one), and we impose the 40% poles of lowest frequencies when the identification technique allows it. We define models of variable order that can be stable or unstable in order to study the methods presented above in a broad range of situations. In the second scenario, the methods are applied to aeroelastic data generated using FEM and DLM models as described in section II. This is the primary intended objective of this work, but in this situation, the model used to generate data is fixed. The underlying aeroelastic model can be considered of infinite order because the aerodynamic forces are not rational functions of the frequency. The imposed modes associated to the aeroelastic data are all stable.

The main metric used in the results is the normalized approximation error of the frequency response, defined by

$$error_{response} = \sqrt{\frac{\sum_{k=1}^{N_f} \|H^{true}(e^{j\omega_k}) - H^{ident}(e^{j\omega_k})\|_F^2}{\sum_{k=1}^{N_f} \|H^{true}(e^{j\omega_k})\|_F^2}} \tag{53}$$

where H^{true} and H^{ident} are the true and identified transfer functions respectively, N_f is the number of data points, and $\|.\|_F$ indicates the Frobenius norm.

The state-space model used to generate the test data in section VII.B has 7 outputs and 11 inputs. It contains poles with the same damping ratio of 0.1 and frequencies linearly ranging from 0.1 Hz to 5 Hz. The frequency data is computed at 200 different frequencies, linearly ranging from 0 Hz to 10 Hz. The aeroelastic data are obtained from a XRF1-HARW model designed by Airbus and University of Michigan. The aeroelastic data response is obtained at Mach 0.85 and altitude 9000 m (from which the density is obtained using the standard atmosphere model), and the aircraft is empty (no fuel and no payload) with a center of gravity position at about 25% of the mean aerodynamic chord, aft of the

Identification method	Reference section	Continuous/ discrete time	Numerical operations	Imposed poles	Constrained free poles	Approximation error	Computational time
Subspace	III.A	Discrete	Linear algebra	No	No	Very low	Few seconds
Loewner	III.B	Continuous	Linear algebra	No	No	Very low	Few seconds
Stable subspace	IV	Discrete	Convex optimization	No	Yes	Very low	Few seconds
SIDORT	V	Discrete	Linear algebra	Yes	No	High	Few seconds
SIDPEV	VI.A	Discrete	Nonlinear optimization	Yes	Yes	Low	Minutes/hours
DNOC	VI.B	Discrete	Nonlinear optimization	Yes	Yes	Low	Hours

Table 1 Summary of the different identification methods

leading edge. Only the longitudinal dynamics are considered. The aeroelastic data include 7 outputs (pitch angle, pitch velocity, vertical load factor, shear force, bending moment and torsional moment at wing root) and 25 inputs (one pair of elevators and 24 pairs of ailerons). The frequency response is computed at 300 different frequencies linearly ranging from 0 Hz to 10 Hz. Initially 80 structural modes are included in the FEM model, in addition to the 6 rigid modes. The number of longitudinal modes with frequency below 10 Hz is about 20. Seven pairs of conjugated aeroelastic poles are imposed in addition to an integrator, when the method allows it. They are chosen as those contributing the most to the transfer function of the considered input/output pairs. Note that the aeroelastic response is normalized before being used by the different identification algorithms, in such a way that all inputs and outputs have approximately the same weight in the identification process.

In the nonlinear subspace method (SIDPEV) defined in VI.A, minimum singular values of 10^{-7} are accepted in the nonlinear constraint definition. Up to 10 runs with different initializations are performed for each optimization as long as the objective function has not reached a threshold of 10^{-7}. A maximum of 1000 function evaluations is set for the direct method defined in VI.B. Both methods are implemented using an interior-point algorithm [48, 49] in which the gradient of the objective function with respect to the parameters is computed and supplied.

A summary of the different methods investigated in this work is shown in Table 1. Their accuracy and computational time are given to give an approximate order of magnitude. For example, to identify a 60th order reduced model with 11 inputs and 7 outputs, the SIDPEV methods takes about 16 minutes, the DNOC 2 hours, and the other methods between 5 and 20 seconds. The computational complexity will be studied more accurately in the following results.

B. Results with test data (first scenario)

In this section, the first scenario described in sections VII.A is tested. In Fig. 2, the amplitude of the transfer function associated to a pair of input/output of the true test data is shown in solid line. On the left part of the figure, the different identification techniques presented in this paper are applied to obtain models of same order as the model used to generate the test data (40), and the amplitude of the difference between the test data and the identified frequency response is shown in dotted line. Note the difference between the dotted lines, which represent approximation errors,

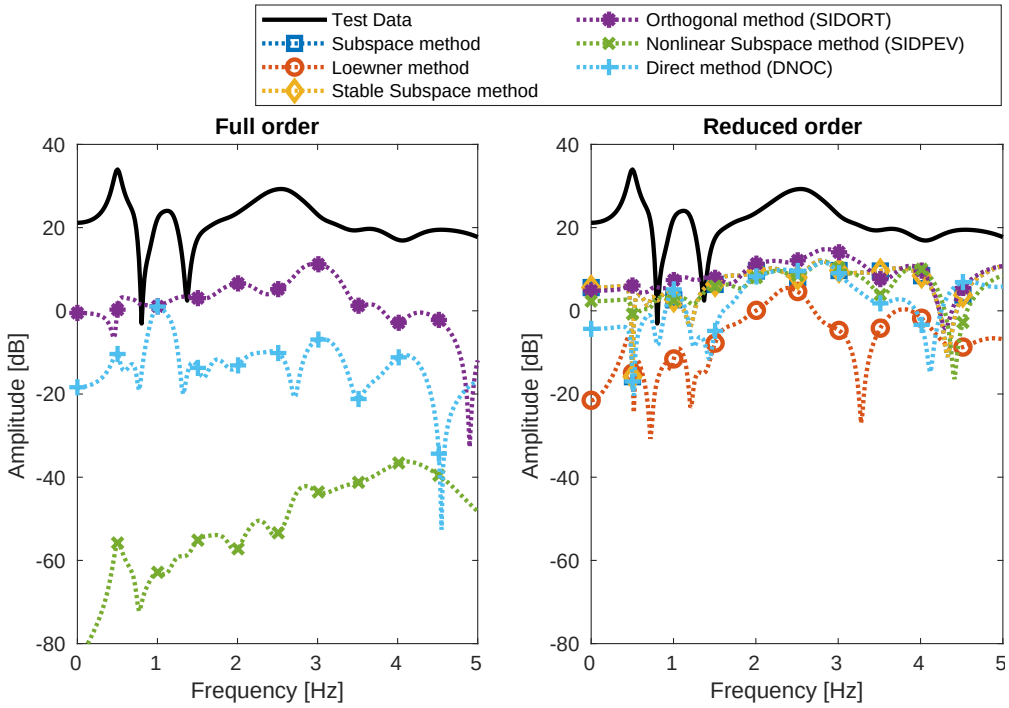

Figure 2 Amplitude of the test data (solid line) and of the approximation errors with different methods (dotted line) with 40th-order (left, same as the state-space used to generate test data) and 30-th order (right) models

and the solid line, which is reported to show the response from the data. The lines that are not represented are below the figure's window, we consider that in this case the approximation is perfect. It results from this figure that the Loewner and subspace methods (with and without stability constraint) approximate the underlying system's response with very high accuracy when the order matches. The SIDPEV method leads to a very low error, while the SIDORT and DNOC methods identify the model with a non-zero error, that remains very low when compared to the true response. When looking at the bode diagram with models of reduced order 30 on the right part of Fig. 2, the difference between the different methods is less significant, only the Loewner method leads to a better approximation of the test data.

This trend is further investigated in Fig. 3 in which the normalized approximation error defined in Eq. (53) is compared for the different presented methods, with variable reduced order and test data generated using a 40-th order state-space model. In the left part, the test data are obtained from a stable model, hence the stability constraints included in some methods (stable subspace, SIDPEV and DNOC) are not expected to increase the approximation error. It can be seen that the Loewner method, the subspace algorithms (with and without stability constraint) and the SIDPEV method have the same trend, with a decreasing approximation error as the reduced order increases, and close to zero when the order of the underlying model is reached. This validates the SIDPEV method, in which nonlinear optimization issues (such as local minimum) do not seem to alter the results. The direct optimization method DNOC is more efficient at low reduced order, but does not perfectly approximate the transfer function response at full order and above. Note that

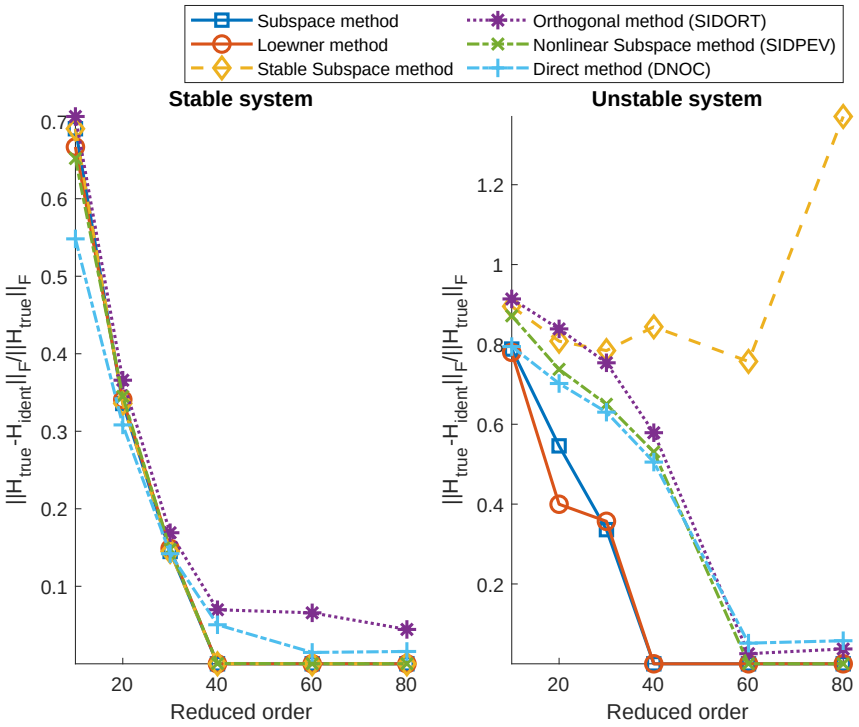

Figure 3 Approximation error with models of different reduced orders (the test data are generated using a 40th order model), in case all poles are stable (left) and half of the poles are unstable (right)

this method is greatly affected by the number of iterations of the nonlinear optimization. For the sake of applicability, it is limited to 1000 but theoretically with a higher computational time, lower errors would be obtained at full order and above. Finally, the SIDORT method has a slightly higher error, due to the additional constraint of orthogonality between the identified and the imposed poles. The SIDORT method is validated by this experience at it leads to errors comparable to the well-established subspace and Loewner method at reduced-order. On the right part of Fig. 3, the same experience is done with test data generated from a state-space model with half of the poles unstable. The Loewner and unconstrained subspace methods lead to results similar to the stable case. The SIDPEV and DNOC methods have stability constraints in the free poles location, which expectedly leads to an increased approximation error. In the case of SIDPEV and DNOC, the model eventually approximates the true test data with good accuracy with a reduced order of 60 and above. In the case of the stable subspace, the constraints is stronger that with SIDPEV and DNOC as no pole is imposed, hence all poles of the identified model are stable. This explains the higher errors obtained with the stable subspace method, and illustrates how imposing unstable poles can improve the approximation when the free poles must be stable. Finally the SIDORT leads to approximation errors similar to the methods with constrained poles.

In Fig. 4 the case in which the identified models are of the same order as the state-space model that generates the test data, is further investigated. For different values of this order, the capability of the presented methods to approximate the frequency response is evaluated. This aims at verifying that no numerical issue arise when the order increases. Indeed,

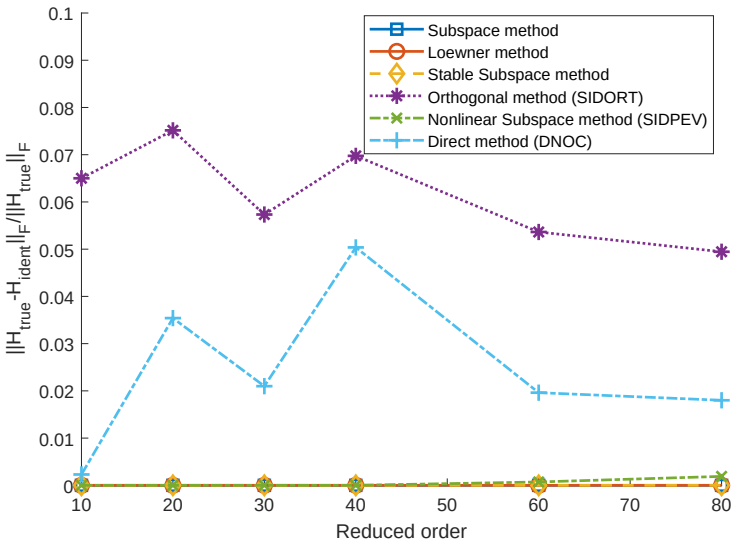

Figure 4 Approximation error with models of the same order as the state-space used to generate test data

not only this causes the matrices' size (such as the observability matrix) to increase, but also the number of variables in the SIDPEV and DNOC. In Fig. 4 the Loewner and subspace (with and without stability constraint) methods lead to very low approximation error, regardless of the order. Considering the SIDPEV method, the error remains very low, although a slight increase seems to start at order 80. In the range of reduced orders of interest for this work, no numerical issue exist with the SIDPEV method. Similarly, the error obtained with the SIDORT method remains low at high orders, and even tends to decrease.

To conclude the comparison and validation of the presented methods on the test data, the computation time is studied. On Fig. 5, the time needed to perform the identification is shown with the different methods. The DNOC method, that relies on a nonlinear optimization with constraints and a high number of parameters, leads to the highest computation time. It lasts more than one hour when the reduced order is higher than 40. Note that by increasing the maximum number of iterations, this time would increase and the approximation error would be lower at higher orders. The SIDPEV methods starts having computational time comparable to the DNOC when the order approaches 80. The other techniques are much faster, as seen on Fig. 5. Up to the order 40, the computation time is lower than 40 s for all techniques except the DNOC. The Loewner method is slightly slower than the subspace methods. The convex optimization used in the stable subspace method proves its efficiency compared to nonlinear optimization-based algorithm, in terms of computational time. Finally, the SIDORT method manages to perform a hybrid identification with some imposed poles in a relatively short time. For the sake of conciseness, the influence of the number of inputs and outputs is not shown in these results. A quick consideration can be made concerning the unconstrained subspace Loewner methods, assuming that the most time-consuming operation is the SVD. In both cases, the decomposition is performed on matrices ($\mathcal{H}\mathcal{U}^{\perp}$ for the subspace method and $\begin{bmatrix}\mathbb{L} & \mathbb{L}_{\sigma}\end{bmatrix}$ for the Loewner method) which scale linearly

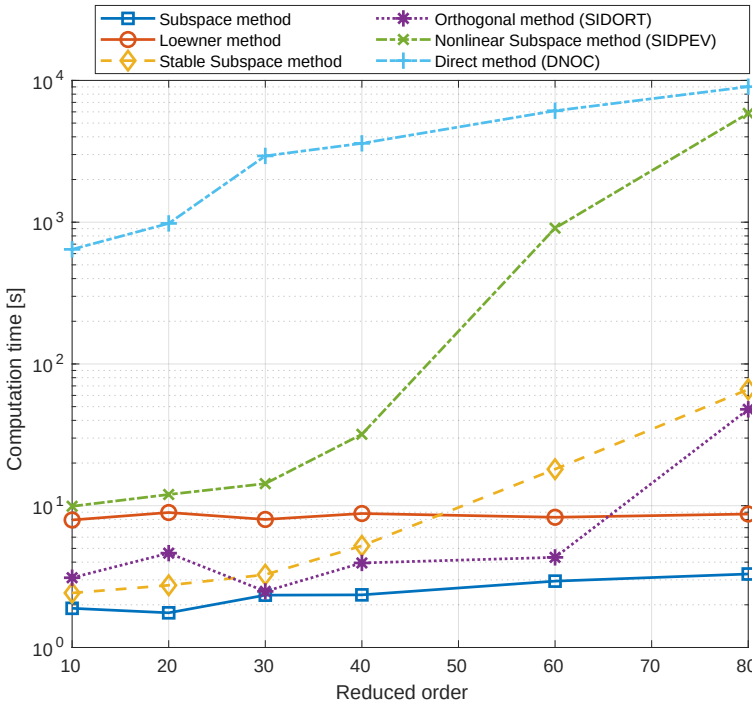

Figure 5 Computation time of the identification techniques

with N_y and N_u in number of rows and columns respectively. The SVD having a time complexity of $O(\min(mn^2, m^2n))$ with m and n the number of rows and columns of the matrix to decompose, the time complexity of the unconstrained algorithm approximately follows $O(\min(N_y N_u^2, N_y^2 N_u))$.

C. Results with aeroelastic data (second scenario)

This section presents the second scenario in which the true data come from an aeroelastic model described in section II with additional details in sections VII.A. Contrary to the test data used in the previous section, the aeroelastic data are not generated by a finite-order transfer function or state-space model, hence the objective is to approximate it with the best accuracy possible. Furthermore, as explained in section II, the poles that we wish to impose are not perfectly known, they result from an estimation using the p-k method.

In Fig. 6, the amplitude of the aeroelastic transfer function from the wind velocity and elevator deflection to the vertical load factor and wing root bending moment is shown in solid line, for frequencies ranging from 0 Hz to 5 Hz. All values are normalized. Similarly to the previous section, the different identification methods defined in this work are compared and the amplitudes of the difference between the 40-th order identified models and the true frequency data are plotted in dotted lines. All methods lead to errors that are significantly lower than the true response. The Loewner method is by far the most accurate, and performs better than the subspace method in this situation. The stable subspace method with stability constraint leads to an error comparable to the subspace method obtained without

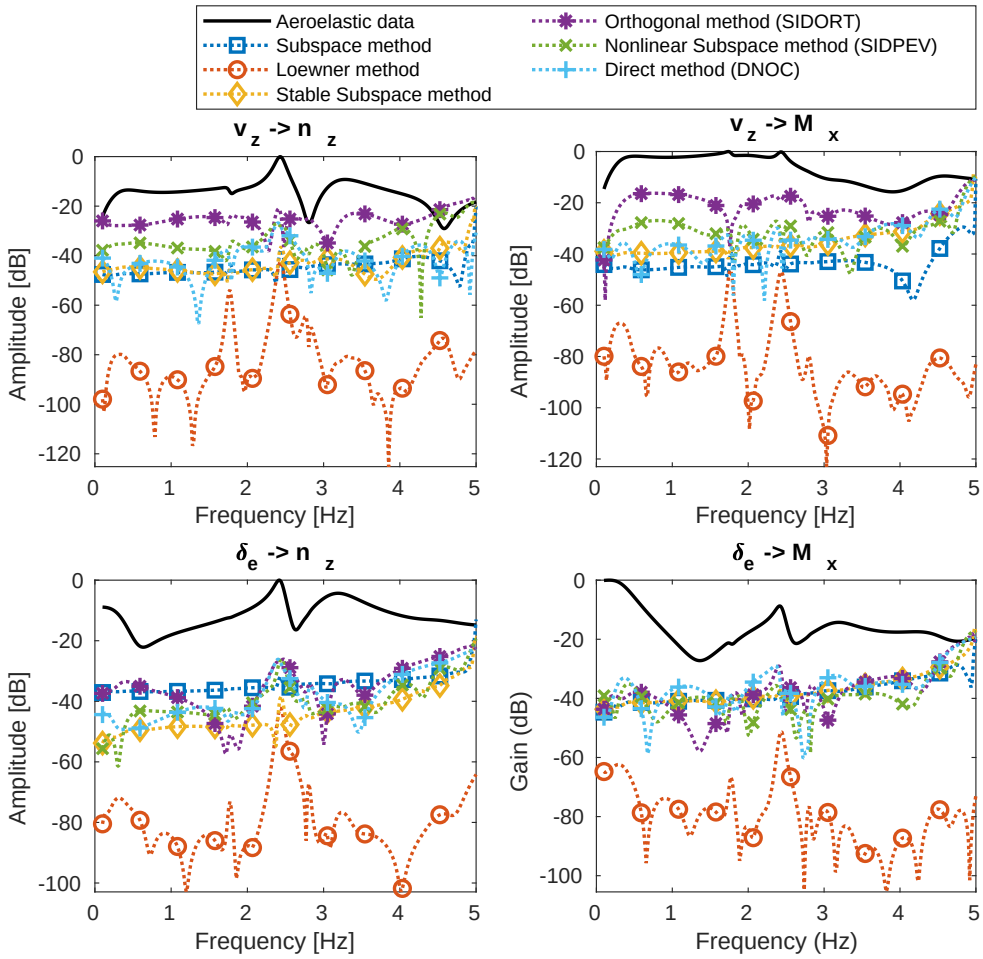

Figure 6 Amplitude of the aeroelastic data (solid line) and of the approximation errors with different methods (dotted line) with 40-th order models, from vertical wind velocity (v_z) and elevator deflection (δ_e) inputs to vertical load factor (n_z) and wing root bending moment (M_x) outputs

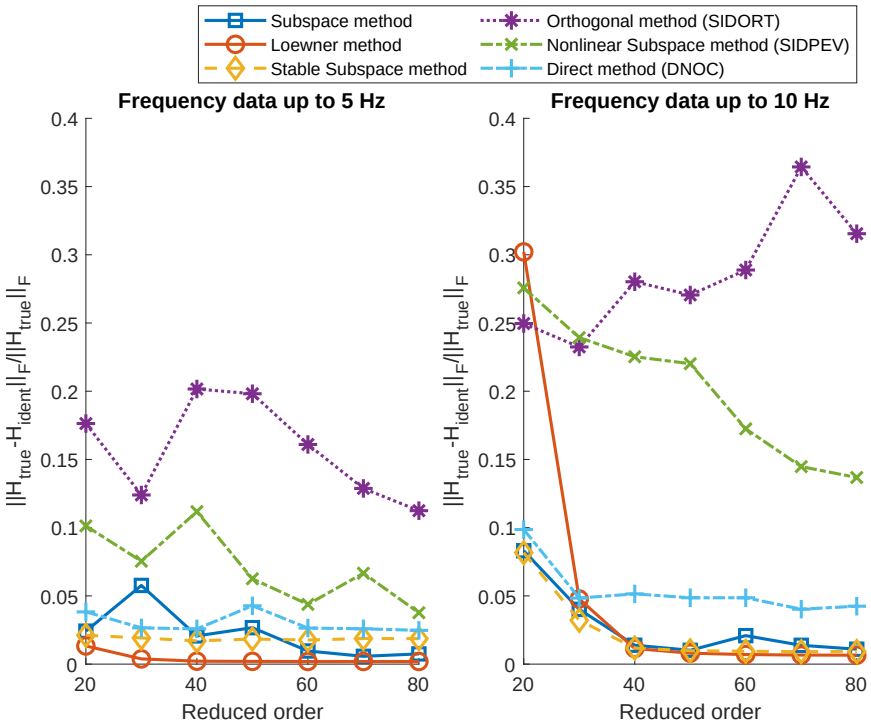

Figure 7 Approximation error with models of different reduced orders, with aeroelastic data up to 5 Hz (left) and 10 Hz (right)

constraints. When imposing some aeroelastic poles, the SIDPEV and DNOC methods lead to a good approximation of the aeroelastic transfer function, while the SIDORT method is slightly less accurate.

More complete results are presented on the left part of Fig. 7, where the normalized errors of Eq. (53) are computed with models of different reduced orders. The global trend is a reduction of the error when the reduced-order increases. Some methods, such as the stable subspace method and the DNOC, show an error that does not decrease when the order increases. It can also be noted that the methods relying on nonlinear optimization (SIDPEV and DNOC) show relatively continuous results. Although a proper analysis would be needed to confirm it, this tends to show that they always converge to satisfactory results. A final observation concerns the SIDORT method, for which the best results are obtained at order 30, a higher order leads to a higher error. Although no numerical issue has been detected with the analysis of the previous section, this shows that the reduced order should be chosen with care when using this method, requiring an a-priori knowledge of the approximative underlying system's order. The left part of Fig. 7 shows the same analysis, but performed with data up to 10 Hz instead of 5 Hz. This increases the complexity of the system, as more modes are involved in the frequency response. Note that the number of imposed poles is the same as in the previous case. It can be seen that the methods require a higher order to converge to the asymptotic error. In this case, the advantage of the Loewner method is less marked, and the stable subspace method still leads to a low error while imposing stability. The SIDPEV method still leads to a low error, that decreases when the order increases. The SIDORT

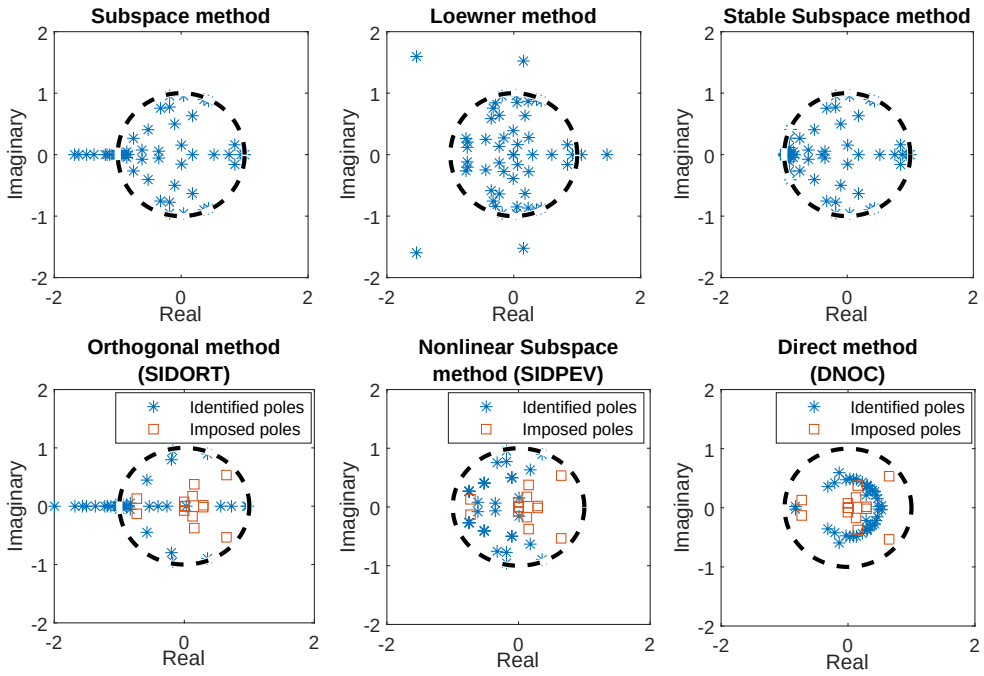

Figure 8 Poles of the identified models obtained by different techniques and imposed poles when applicable

method is less accurate in this case, and the error tends to increase with the order, confirming the fact that the reduced order should be chosen adequately.

Finally, an illustration of the poles locations using the different methods is provided in Fig. 8. These correspond to the discrete-time poles, which are stable when they are located within the unit disk. In case the identified model is continuous (Loewner method only), the poles λ_i are converted to their discrete-time counterpart $e^{T_s \lambda_i}$. It can be seen that the stability is correctly imposed by the stable subspace, SIDPEV and DNOC methods, while the Loewner, subspace and SIDORT methods lead to unstable poles as no constraint is put on them. The pairs of imposed poles are shown for the techniques that impose them. It can be seen that the DNOC method identifies poles with an almost constant modulus, this could correspond to a sub-optimal result from the nonlinear identification.

VIII. Conclusions

In this work, reduced order modeling techniques intended for aeroelastic systems have been presented and tested. The full aeroelastic transfer function corresponding to certain inputs and outputs of interest is identified based on its frequency response. The Loewner method has been applied and compared to a subspace algorithm, in which the possibility to apply constraints on the poles have been studied. Furthermore, in order to improve the physical interpretability of the identified models, dedicated techniques have been developed specifically for this work to impose a set of a-priori known poles that can be stable or unstable. These methods have been compared through different scenarios, starting from stable and unstable models of various orders, to finally be applied to aeroelastic data in which

case the imposed poles have been computed by p-k method beforehand .

It results from this work that the different methods described are valid over the range of reduced orders studied (up to 80). The transfer function response is systematically approximated with an error that remains at least one order of magnitude below the true value, provided the reduced order is high enough. The different constraints (poles location, imposed poles) are successfully applied by the relevant methods.

A first comparison can be performed between McKelvey subspace algorithm and the Loewner interpolation method, when no constraint is applied to the identified models. The Loewner method is slightly slower than the subspace algorithm, but is more efficient at approximating a system with a reduced order. This has been verified using data generated with a fixed-order random state-space model and with an aeroelastic model. Another advantage of the Loewner method is that it leads to a continuous-time model, that can more easily be transformed into a discrete-time state-space of any sampling time if needed. Although not shown in this work for the sake of conciseness, similar conclusions can be drawn with different numbers of inputs and outputs. Furthermore, the stable subspace algorithm based on [40] is able to approximate a transfer function within an error comparable to the McKelvey subspace algorithm and with a similar computational time within the reduced order range considered in this work, whilst ensuring stability. It can hence be applied to obtain models used in simulations and control synthesis without the classical instability issues obtained with the Loewner and subspace methods.

A second comparison concerns the different techniques defined for imposing some poles of the system, with and without constraints on the free poles. The SIDORT method adds very little complexity to the McKelvey algorithm as mainly eigenvalue problems and SVD decomposition concerning matrices of low sizes are concerned in the additional step. However, it suffers from two main limitations: the first is the hypothesis of orthogonality between the eigenvectors associated to the imposed poles and to the free poles respectively. The second is the fact that it does not impose stability of the free poles. It approximates the data with good accuracy but lower than the other techniques presented in the current work. When applied to the aeroelastic data, the error does not seem to systematically decrease as the reduced order increases. It can also be noted that it cannot perfectly approximate the data when the reduced order is the same as the generating model's order, due to the orthogonality constraint. In comparison, the SIDPEV method leads to lower approximation errors both with the test and the aeroelastic data, and although it relies on a nonlinear optimization with constraints that requires multiple runs with different initial conditions, its computational time remains low at orders lower or equal to 40, and always converges to a satisfactory solution. Finally, the DNOC method relies on an direct optimization to find the state-space matrices of the reduced order model with constraints on the poles. Because of the high number of variables, this method requires high computational times, but eventually converges to solutions with good approximation accuracy. It can be noted that when the complexity of the system increases (higher order or in case of the aeroelastic data on a broader frequency range), the number of iterations required to converge increases. For practical use, when poles must be imposed to the identified model, the SIDPEV method seems the most appropriate.

Some remarks about the limits of this study can be formulated to prepare future works. Concerning the choice of working with frequency response of the full aeroelastic transfer function, it must be noted that a different identification must be performed for each mass configuration and aerodynamic (Mach number, altitude), with no possibility of using a common structure. Furthermore, imposing some known poles to the identified model does not mean that they will have the same effect on the transfer function as in the true system. This could be quantified by defining the pole-residue decomposition of a transfer function H in the z-domain as

$$H(z) = \sum_{i=1}^{n} \frac{R_i}{z - \lambda_i} \tag{54}$$

where the residues $R_i \in \mathbb{C}^{N_y \times N_u}$ associated to the poles λ_i give an idea of how they affect the transfer function, and methods based on this principle could be developed so that the imposed poles have a similar behavior as in the true system. A second remark concerns the complexity of the algorithms. In this work only models of limited sizes evaluated on relatively low amounts of data have been considered, and numerical issues such as memory limitations could happen with bigger systems. Finally, while efforts have been done to improve the convergence of the DNOC algorithm, different optimization schemes could be studied in order to converge to better solutions in shorter times.

Acknowledgments

This work has been funded by Airbus Operations SAS and the French National Agency for Technological Research (ANRT) under grant number 2019/1611. This support is gratefully appreciated.

Appendix

A. Recovering the D-term with the Loewner method

As explained in section III.B, the Loewner method leads to a continuous-time descriptor model described in Eq. (32). In case the system is causal, the descriptor model can be transformed into a classical continuous-time state-space model composed of matrices A, B, C and D. We propose a procedure to recover this state-space formulation in the case the system is causal and does not include integrators. This can be justified by the fact that in case an integrator is present, the low-frequency response will tend to infinity for some input/output pairs, leading to ill-conditioned Loewner matrices. If the data does not include low frequencies, then the response will not be infinite, and the integrator can be approximated by a low-frequency pole. Then, the proposed procedure is valid even in presence of an integrator, as long as frequency data are not too low.

We start by finding the generalized eigenvalues of the matrices $E \in \mathbb{R}^{n \times n}$ and $A \in \mathbb{R}^{n \times n}$ obtained from the Loewner method:

$$EP = AP\Lambda \tag{55}$$

where $P \in \mathbb{C}^{n\times n}$ is a real invertible matrix and $\Lambda \in \mathbb{C}^{n\times n}$ is diagonal with generalized eigenvalues of (E, A). Note that P can easily be converted to a real matrix, and Λ to a real block-diagonal matrix of the form of Eq. (51) to obtain the modal form. The generalized eigenvalues correspond to the inverse of the poles of the descriptor system. The reason for not working directly with the poles of the system is that the D term is associated to poles of the system with infinite modulus, hence the inverse have zero values.

We apply a variable substitution in Eq. (32) by writing $x = P\xi$, which leads to:

$$\begin{cases} EP\dot{\xi} = AP\Lambda\dot{\xi} = AP\xi + Bu \\ y = CP\xi \end{cases} \tag{56}$$

which is the modal form of the system. We then split the poles between those with nonzero values and those with zero values:

$$\Lambda = \begin{bmatrix} \Lambda_1 & 0 \\ 0 & 0 \end{bmatrix}, \qquad \xi = \begin{bmatrix} \xi_1 \\ \xi_2 \end{bmatrix}, \qquad P = \begin{bmatrix} P_1 & P_2 \end{bmatrix}, \qquad P^{-1} = \begin{bmatrix} P_1^{inv} \\ P_2^{inv} \end{bmatrix} \tag{57}$$

Since by assumption the system does not include integrators, the matrix A is invertible and so is AP since P is full rank. We can then rewrite the first equation of (56) as

$$\Lambda\dot{\xi} = \xi + (AP)^{-1}Bu \tag{58}$$

By taking the first rows of Eq. (58), associated to the non-zero generalized eigenvalues, we obtain the state equation:

$$\dot{\xi}_1 = \Lambda_1^{-1}\xi_1 + \Lambda_1^{-1}P_1^{inv}A^{-1}Bu \tag{59}$$

where Λ_1 is invertible since it contains only the nonzero values of Λ. By taking the last rows of Eq. (58), we obtain a second equation that connects ξ_2 to u:

$$0 = \xi_2 + P_2^{inv}A^{-1}Bu \tag{60}$$

By injecting into the output equation of Eq. (56), we obtain:

$$y = CP_1\xi_1 + CP_2\xi_2 = CP_1\xi_1 - CP_2P_2^{inv}A^{-1}Bu \tag{61}$$

This concludes the definition of a state-space model (A', B', C', D') with matrices:

$$A' = \Lambda_1^{-1}, \qquad B' = \Lambda_1^{-1}P_1^{inv}A^{-1}B, \qquad C' = CP_1, \qquad D' = -CP_2P_2^{inv}A^{-1}B \tag{62}$$

References

[1] Bisplinghoff, R., Ashley, H., and Halfman, R., *Aeroelasticity*, Addison-Wesley Publishing Company, 1955, pp. 632–641.

[2] Etkin, B., *Dynamics of Flight – Stability and Control*, Wiley, New York, 1959, pp. 120–126.

[3] Lucia, D. J., Beran, P. S., and Silva, W. A., "Reduced-order modeling: new approaches for computational physics," *Progress in Aerospace Sciences*, Vol. 40, No. 1, 2004, pp. 51–117. https://doi.org/https://doi.org/10.1016/j.paerosci.2003.12.001, URL https://www.sciencedirect.com/science/article/pii/S0376042103001131.

[4] Stalford, H., Baumann, W. T., Garrett, F. E., and Herdman, T. L., "Accurate Modeling of Nonlinear Systems using Volterra Series Submodels," *1987 American Control Conference*, 1987, pp. 886–891. https://doi.org/10.23919/ACC.1987.4789437.

[5] Jenkins, J. E., *Relationships among nonlinear aerodynamic indicial response models, oscillatory motion data, and stability derivatives*, 1989. https://doi.org/10.2514/6.1989-3351, URL https://arc.aiaa.org/doi/abs/10.2514/6.1989-3351.

[6] Hall, K. C., Thomas, J. P., and Dowell, E. H., "Proper Orthogonal Decomposition Technique for Transonic Unsteady Aerodynamic Flows," *AIAA Journal*, Vol. 38, No. 10, 2000, pp. 1853–1862. https://doi.org/10.2514/2.867, URL https://doi.org/10.2514/2.867.

[7] Romanowski, M., and Dowell, E., *Aeroelastic analysis of an airfoil using eigenmode based reduced order unsteady aerodynamics*, 1995. https://doi.org/10.2514/6.1995-1380, URL https://arc.aiaa.org/doi/abs/10.2514/6.1995-1380.

[8] Kim, T., "Frequency-Domain Karhunen-Loeve Method and Its Application to Linear Dynamic Systems," *AIAA Journal*, Vol. 36, No. 11, 1998, pp. 2117–2123. https://doi.org/10.2514/2.315, URL https://doi.org/10.2514/2.315.

[9] Thomas, J. P., Dowell, E. H., and Hall, K. C., "Nonlinear Inviscid Aerodynamic Effects on Transonic Divergence, Flutter, and Limit-Cycle Oscillations," *AIAA Journal*, Vol. 40, No. 4, 2002, pp. 638–646. https://doi.org/10.2514/2.1720, URL https://doi.org/10.2514/2.1720.

[10] Huang, R., Hu, H., and Zhao, Y., "Nonlinear Reduced-Order Modeling for Multiple-Input/Multiple-Output Aerodynamic Systems," *AIAA Journal*, Vol. 52, No. 6, 2014, pp. 1219–1231. https://doi.org/10.2514/1.J052323, URL https://doi.org/10.2514/1.J052323.

[11] Lee-Rausch, E. M., and Batina, J. T., "Wing flutter computations using an aerodynamic model based on the Navier-Stokes equations," *Journal of Aircraft*, Vol. 33, No. 6, 1996, pp. 1139–1147. https://doi.org/10.2514/3.47068, URL https://doi.org/10.2514/3.47068.

[12] Waszak, M. R., and Schmidt, D. K., "Flight dynamics of aeroelastic vehicles," *Journal of Aircraft*, Vol. 25, No. 6, 1988, pp. 563–571. https://doi.org/10.2514/3.45623, URL https://doi.org/10.2514/3.45623.

[13] Schmidt, D. K., and Raney, D. L., "Modeling and Simulation of Flexible Flight Vehicles," *Journal of Guidance, Control, and Dynamics*, Vol. 24, No. 3, 2001, pp. 539–546. https://doi.org/10.2514/2.4744, URL https://doi.org/10.2514/2.4744.

[14] Reschke, C., "Flight loads analysis with inertially coupled equations of motion," *AIAA Atmospheric Flight Mechanics Conference and Exhibit*, 2005. https://doi.org/10.2514/6.2005-6026.

[15] Guimarães Neto, A. B., Silva, R. G. A., Paglione, P., and Silvestre, F. J., "Formulation of the Flight Dynamics of Flexible Aircraft Using General Body Axes," *AIAA Journal*, Vol. 54, No. 11, 2016, pp. 3516–3534. https://doi.org/10.2514/1.J054752, URL https://doi.org/10.2514/1.J054752.

[16] Patil, M. J., and Hodges, D. H., "Flight Dynamics of Highly Flexible Flying Wings," *Journal of Aircraft*, Vol. 43, No. 6, 2006, pp. 1790–1799. https://doi.org/10.2514/1.17640, URL https://doi.org/10.2514/1.17640.

[17] Su, W., and Cesnik, C. E. S., "Nonlinear Aeroelasticity of a Very Flexible Blended-Wing-Body Aircraft," *Journal of Aircraft*, Vol. 47, No. 5, 2010, pp. 1539–1553. https://doi.org/10.2514/1.47317, URL https://doi.org/10.2514/1.47317.

[18] Fournier, H., Massioni, P., Tu Pham, M., Bako, L., Vernay, R., and Colombo, M., "Robust Gust Load Alleviation of Flexible Aircraft Equipped with Lidar," *Journal of Guidance, Control, and Dynamics*, Vol. 45, No. 1, 2022, pp. 58–72. https://doi.org/10.2514/1.G006084, URL https://doi.org/10.2514/1.G006084.

[19] Fournier, H., Massioni, P., Pham, M. T., Bako, L., Vernay, R., and Colombo, M., *Robust Gust Load Alleviation at Different Flight Points and Mass configurations*, 2022. https://doi.org/10.2514/6.2022-0285, URL https://arc.aiaa.org/doi/abs/10.2514/6.2022-0285.

[20] Livne, E., "Aircraft Active Flutter Suppression: State of the Art and Technology Maturation Needs," *Journal of Aircraft*, Vol. 55, No. 1, 2018, pp. 410–452. https://doi.org/10.2514/1.c034442.

[21] Ustinov, A., Sidoruck, M., and Goman, M., "Control Law Design for Flexible Aircraft: Comparison of the H-Infinity-based and Classical Methods," *AIAA Guidance, Navigation, and Control Conference and Exhibit*, American Institute of Aeronautics and Astronautics, 2005. https://doi.org/10.2514/6.2005-6265.

[22] Luspay, T., Ossmann, D., Wuestenhagen, M., Teubl, D., Baár, T., Pusch, M., Kier, T. M., Waitman, S., Ianelli, A., Marcos, A., Vanek, B., and Lowenberg, M. H., "Flight control design for a highly flexible flutter demonstrator," *AIAA Scitech 2019 Forum*, American Institute of Aeronautics and Astronautics, 2019. https://doi.org/10.2514/6.2019-1817.

[23] Albano, E., and Rodden, W. P., "A doublet-lattice method for calculating lift distributions on oscillating surfaces in subsonic flows." *AIAA Journal*, Vol. 7, No. 2, 1969, pp. 279–285. https://doi.org/10.2514/3.5086, URL https://doi.org/10.2514/3.5086.

[24] Kalman, T. P., Rodden, W. P., and Giesling, J. P., "Application of the Doublet-Lattice Method to Nonplanar Configurations in Subsonic Flow," *Journal of Aircraft*, Vol. 8, No. 6, 1971, pp. 406–413. https://doi.org/10.2514/3.59117, URL https://doi.org/10.2514/3.59117.

[25] Konstadinopoulos, P., Thrasher, D. F., Mook, D. T., Nayfeh, A. H., and Watson, L., "A vortex-lattice method for general, unsteady aerodynamics," *Journal of Aircraft*, Vol. 22, No. 1, 1985, pp. 43–49. https://doi.org/10.2514/3.45078, URL https://doi.org/10.2514/3.45078.

[26] Hesse, H., and Palacios, R., "Reduced-Order Aeroelastic Models for Dynamics of Maneuvering Flexible Aircraft," *AIAA Journal*, Vol. 52, No. 8, 2014, pp. 1717–1732. https://doi.org/10.2514/1.J052684, URL https://doi.org/10.2514/1.J052684.

[27] Hesse, H., and Palacios, R., "Dynamic Load Alleviation in Wake Vortex Encounters," *Journal of Guidance, Control, and Dynamics*, Vol. 39, No. 4, 2016, pp. 801–813. https://doi.org/10.2514/1.G000715, URL https://doi.org/10.2514/1.G000715.

[28] Roger, K., "Airplane Math Modeling Methods for Active Control Design," *AGARD-CP-228*, 1977, pp. 1–11.

[29] Karpel, M., "Design for Active Flutter Suppression and Gust Alleviation Using State-Space Aeroelastic Modeling," *Journal of Aircraft*, Vol. 19, No. 3, 1982, pp. 221–227. https://doi.org/10.2514/3.57379, URL https://doi.org/10.2514/3.57379.

[30] Waite, J., Stanford, B., Bartels, R. E., Silva, W. A., and Massey, S. J., *Active Flutter Suppression Controllers Derived from Linear and Nonlinear Aerodynamics: Application to a Transport Aircraft Model*, 2018. https://doi.org/10.2514/6.2018-2836, URL https://arc.aiaa.org/doi/abs/10.2514/6.2018-2836.

[31] Juang, J.-N., and Pappa, R. S., "An eigensystem realization algorithm for modal parameter identification and model reduction," *Journal of Guidance, Control, and Dynamics*, Vol. 8, No. 5, 1985, pp. 620–627. https://doi.org/10.2514/3.20031, URL https://doi.org/10.2514/3.20031.

[32] Silva, W., and Raveh, D., "Development of Unsteady Aerodynamic State-Space Models from CFD-Based Pulse Responses," *19th AIAA Applied Aerodynamics Conference*, 2001. https://doi.org/10.2514/6.2001-1213.

[33] Silva, W. A., "AEROM: NASA's Unsteady Aerodynamic and Aeroelastic Reduced-Order Modeling Software," *Aerospace*, Vol. 5, No. 2, 2018. https://doi.org/10.3390/aerospace5020041, URL https://www.mdpi.com/2226-4310/5/2/41.

[34] Waite, J., Stanford, B., Bartels, R. E., and Silva, W. A., "Active Flutter Suppression Using Reduced Order Modeling for Transonic Aeroservoelastic Control Law Development," *AIAA Aviation 2019 Forum*, 2019. https://doi.org/10.2514/6.2019-3025, URL https://arc.aiaa.org/doi/abs/10.2514/6.2019-3025.

[35] Green, M., "A relative error bound for balanced stochastic truncation," *IEEE Transactions on Automatic Control*, Vol. 33, No. 10, 1988, pp. 961–965. https://doi.org/10.1109/9.7255.

[36] Qin, S. J., "An overview of subspace identification," *Computers and Chemical Engineering*, Vol. 30, No. 10, 2006, pp. 1502–1513. https://doi.org/https://doi.org/10.1016/j.compchemeng.2006.05.045, URL https://www.sciencedirect.com/science/article/pii/S009813540600158X, papers form Chemical Process Control VII.

[37] Mayo, A., and Antoulas, A., "A framework for the solution of the generalized realization problem," *Linear Algebra and its Applications*, Vol. 425, No. 2-3, 2007, pp. 634–662. https://doi.org/10.1016/j.laa.2007.03.008.

[38] Karachalios, D., Gosea, I., and Antoulas, A., *The Loewner framework for system identification and reduction*, De Gruyter, 2019. https://doi.org/10.1515/9783110498967-006.

[39] Kergus, P., Formentin, S., Poussot-Vassal, C., and Demourant, F., "Data-driven control design in the Loewner framework: Dealing with stability and noise," *2018 European Control Conference (ECC)*, 2018, pp. 1704–1709. https://doi.org/10.23919/ECC.2018.8550216.

[40] Miller, D. N., and De Callafon, R. A., "Subspace Identification with Eigenvalue Constraints," *Automatica*, Vol. 49, No. 8, 2013, p. 2468–2473. https://doi.org/10.1016/j.automatica.2013.04.028, URL https://doi.org/10.1016/j.automatica.2013.04.028.

[41] Chilali, M., and Gahinet, P., "H-infinity Design with Pole Placement Constraints: an LMI Approach," *Automatic Control, IEEE Transactions on*, Vol. 41, 1996, pp. 358 – 367. https://doi.org/10.1109/9.486637.

[42] Lacy, S., and Bernstein, D., "Subspace identification with guaranteed stability using constrained optimization," *IEEE Transactions on Automatic Control*, Vol. 48, No. 7, 2003, pp. 1259–1263. https://doi.org/10.1109/TAC.2003.814273.

[43] Hassig, H., "An approximate true damping solution of the flutter equation by determinant iteration." *Journal of Aircraft*, Vol. 8, No. 11, 1971, pp. 885–889. https://doi.org/10.2514/3.44311, URL https://doi.org/10.2514/3.44311.

[44] Tang, W., Wu, J., and Shi, Z., "Identification of reduced-order model for an aeroelastic system from flutter test data," *Chinese Journal of Aeronautics*, Vol. 30, No. 1, 2017, pp. 337–347. https://doi.org/https://doi.org/10.1016/j.cja.2016.12.024, URL https://www.sciencedirect.com/science/article/pii/S1000936116302448.

[45] McKelvey, T., Akcay, H., and Ljung, L., "Subspace-based multivariable system identification from frequency response data," *IEEE Transactions on Automatic Control*, Vol. 41, No. 7, 1996, pp. 960–979. https://doi.org/10.1109/9.508900.

[46] Antoulas, A. C., Lefteriu, S., and Ionita, A. C., *Chapter 8: A Tutorial Introduction to the Loewner Framework for Model Reduction*, 2017, pp. 335–376. https://doi.org/10.1137/1.9781611974829.ch8, URL https://epubs.siam.org/doi/abs/10.1137/1.9781611974829.ch8.

[47] Köhler, M., "On the closest stable descriptor system in the respective spaces RH2 and RH-infinity," *Linear Algebra and its Applications*, Vol. 443, 2014, pp. 34–49. https://doi.org/https://doi.org/10.1016/j.laa.2013.11.012, URL https://www.sciencedirect.com/science/article/pii/S002437951300709X.

[48] Byrd, R. H., Hribar, M. E., and Nocedal, J., "An Interior Point Algorithm for Large-Scale Nonlinear Programming," *SIAM Journal on Optimization*, Vol. 9, No. 4, 1999, pp. 877–900. https://doi.org/10.1137/S1052623497325107, URL https://doi.org/10.1137/S1052623497325107.

[49] Waltz, R., Morales, J., Nocedal, J., and Orban, D., "An interior algorithm for nonlinear optimization that combines line search and trust region steps," *Math. Program.*, Vol. 107, 2006, pp. 391–408. https://doi.org/10.1007/s10107-004-0560-5.